Journal of Hydrology 403 (2011) 103–115

Contents lists available at ScienceDirect

Journal of Hydrology

journal homepage: www.elsevier.com/locate/jhydrol

Calibration of floodplain roughness and estimation of flood discharge based on tree-ring evidence and hydraulic modelling

J.A. Ballesteros [a,*], J.M. Bodoque [b], A. Díez-Herrero [a], M. Sanchez-Silva [c], M. Stoffel [d,e]

[a] Department of Research and Geoscientific Prospective, Geological Survey of Spain (IGME), Ríos Rosas 23, Madrid E-28003, Spain
[b] Mining and Geological Engineering Department, University of Castilla-La Mancha, Campus Fábrica de Armas, Avda. Carlos III, Toledo E-45071, Spain
[c] Department of Civil and Environmental Engineering, Universidad de Los Andes, Bogotá, Colombia
[d] Laboratory of Dendrogeomorphology, Institute of Geological Sciences, University of Berne, 3012 Berne, Switzerland
[e] Climatic Change and Climate Impacts, Environmental Sciences, University of Geneva, 1227 Carouge-Geneva, Switzerland

ARTICLE INFO

Article history:
Received 6 October 2010
Received in revised form 5 March 2011
Accepted 24 March 2011
Available online 2 April 2011

This manuscript was handled by K. Georgakakos, Editor-in-Chief, with the assistance of Purna Chandra Nayak, Associate Editor

Keywords:
Flood
Tree ring
Dendrogeomorphology
Peak discharge estimation
Roughness calibration
Spanish central system

SUMMARY

The roughness calibration of floodplain and channels represents an important issue for flood studies. This paper discusses the genesis of scars on trees and their use as benchmarks in roughness calibration. In addition, it presents a methodology to reconstruct unrecorded flood discharge in the Alberche basin of the Spanish Central System. The study is based on the combined use of dendrogeomorphic evidence (i.e. scars on trees), data from the Navaluenga flow gauge (Avila Province) as well as a 1D/2D coupled numerical hydraulic model. A total of 49 scars have been analyzed with dendrogeomorphic techniques. Scar dates are in concert with seven flood events documented in the systematic record (i.e. 1989, 1993, 1996, 2000, 2002, 2003, and 2005). We were also able to identify an additional event dated to 1970, which is before the flow gauge was installed at Navaluenga. Based on the rating curve obtained from the flow gauge, cross-sectional area and data from hydraulic modelling, we cannot find a statistically significant difference between water depths registered at the flow gauge and scar heights on trees (p-value > 0.05), indicating that scars would have been generated through the impact of floating wood and that scars on trees would represent a valuable and accurate proxy for water depth reconstruction. Under this premise, we have estimated the peak discharge of the 1970 flood event to $1684.3 \pm 519.2\ m^3\ s^{-1}$; which renders this event the largest documented flood for the Alberche River at Navaluenga. In a last analytical step, we discuss the use of scars on trees as benchmark for roughness calibration in ungauged or shortly recorded basins and address the added value of dendrogeomorphic data in flood frequency analysis.

1. Introduction

Developing reliable hydraulic flood models that provide accurate estimates of flood hazards in urban areas are essential to define the best strategies for flood risk mitigation (Enzel et al., 1993; de Kok and Grossmann, 2010). Recently, computational developments have allowed modelling of large and complex floodplains based on the use of 1D/2D coupled hydraulic models (Tayefi et al., 2007; Leandro et al., 2009; Roca et al., 2008) based on Saint–Venant (1D or unsteady 2D flow simulations; Chow, 1959; Souhar and Faure, 2009) as well as Navier–Stokes depth-averaged equations (steady 2D flow simulations; Denlinger et al., 2002; Duan and Nanda, 2006).

Out of all hydraulic parameters involved in the process, roughness coefficients represent, probably, one of the keys for a realistic numerical simulation of open channel flows, but remain especially difficult to determine (Cook, 1987; Kidson et al., 2005; Thorndycraft et al., 2005; Werner et al., 2005; Zhu and Zhang, 2009) as they are influenced by many factors (Chow, 1959; Aldridge and Garrett, 1973). It is estimated that a 50% error in roughness coefficients could imply an error of nearly 40% in peak discharge estimation (Kidson et al., 2002; Sudhaus et al., 2008).

For decades, the assignment of roughness coefficients in natural channels has been performed by comparing cross-sectional areas and river profiles with photographs of typical river and creek cross-sections (see: Barnes, 1967; Arcement and Schenider, 1989) or by means of empirical equations (Chow, 1959; Yen, 2002). However, in the case of unrecorded floods that occurred without instrumental recording and where documentary or observational sources are lacking (i.e. palaeohydrology *sensu* Baker, 2008), the assignment of "palaeo-roughness coefficients" represents a major

* Corresponding author. Tel.: +34 913495807.
E-mail addresses: ja.ballesteros@igme.es (J.A. Ballesteros), josemaria.bodoque@uclm.es (J.M. Bodoque), andres.diez@igme.es (A. Díez-Herrero), msanchez@uniandes.edu.co (M. Sanchez-Silva), markus.stoffel@dendrolab.ch (M. Stoffel).

0022-1694/$ - see front matter © 2011 Elsevier B.V. All rights reserved.
doi:10.1016/j.jhydrol.2011.03.045

challenge. Frequently, the approaches used to assign roughness values may have several drawbacks and shortcomings for flood studies. Some of the main difficulties include the characterization of historical floods, which is not always possible due to the lack of visual or written data to infer maximum flood stage. In the case of empirical approaches, difficulties also arise due to limited values of channel gradient or hydraulic radius (Ferguson, 2007, 2010), relative submergence of vegetation and boulders (Bathurst, 1993) or due to the need to define a critical flow (Grant, 1997; Tinkler, 1997; Comiti et al., 2009) which it is not always easy in natural reaches. As a result, the estimation of roughness coefficients necessary for the development and the appropriate use of hydraulic models remains particularly difficult, especially when dealing with (exceptionally) large flood events (Wohl, 1998).

Despite the use of new technologies for assessing the physical roughness parameters in river channel such as Terrestrial Laser Scanners (TLS; Hodge et al., 2009a,b; Heritage and Milan, 2009; Antonarakis et al., 2009) or Light Detection and Range (LiDAR; Casas et al., 2010; Colmenárez et al., 2010), several issues remain: (i) laser beams used for topography are not operational below the water surface, so roughness in the main channel cannot be properly measured in the case of permanent rivers; and (ii) with the exception of bedrock channels, river beds will only represent current roughness conditions, rendering an appropriate estimation of "palaeo-roughness coefficients" impossible.

So far, dendrogeomorphic evidence (i.e. scars on trees; Stoffel et al., 2010) preserved on riparian vegetation has remained an unexplored alternative for roughness calibration and as a palaeostage indicator (PSI; Jarrett and England, 2002; Benito and Thorndycraft, 2004). Dendrogeomorphology benefits from the fact that impacts of past torrential and fluvial activity will be preserved in the growth-ring record of riparian trees (Simon et al., 2004; Stoffel and Wilford, 2011) and that palaeo-events can thus be dated with (sub-) annual resolution (Gottesfeld and Gottesfeld, 1990; St. George and Nielsen, 2003; Stoffel and Beniston, 2006; Ballesteros et al., 2010a,b; Ruiz-Villanueva et al., 2010). Tree-ring records of impacted trees have been used successfully in the past for flood discharge or magnitude estimations of events in high gradient streams (Stoffel, 2010; Ballesteros et al., 2011), but they have never been utilized for the assessment and calibration of floodplain roughness in fluvial systems.

The key for past flood research is the establishment of relations between PSI and high water marks (HWM), thus addressing the question of when the flood hydrograph was generating PSI. Previous research suggests that observed deviations between PSI (i.e. scars on trees) and HWM (i.e. fresh floating wood) are lower in low-gradient (i.e. 0.196 ± 0.03 m; Gottesfeld, 1996 – 0.005 m/m) than in high-gradient streams (i.e. −0.6 to 1.5 m in Yanosky and Jarrett, 2002 – 0.04 m/m; −0.88 to 1.35 m in Ballesteros et al., 2011 – 0.2 m/m). Although more work is required to characterize this relationship and to avoid the influence of possible local effects (Jarrett and England, 2002), it can be assumed that the stream gradient and the type of material available for transport could be the principal factors contributing to inaccuracy in estimations.

The main objective of this paper is to study the genesis of scars on trees and their use for spatial roughness calibration in fluvial channels so as to improve the input data for unrecorded flood discharge estimations based on hydraulic models. To this end, we analyzed 44 riparian trees growing on the banks of the Alberche river in the Spanish Central System. The sampled trees exhibited 49 scars and the distribution of scar heights was checked against water depths measured at the local flow gauge using non-parametric statistical tests. In a final step, based on the calibrated hydraulic model, a flood event reconstructed by dendrogeomorphology and older than the local flow gauge record was modelled using only tree-ring data.

2. Study site

The study area chosen for the dendrogeomorphic analysis and hydraulic modelling is located in a reach where the Alberche river crosses the village of Navaluenga, located in the Eastern Sierra of Gredos (40°24′30″N; 4°42′17″W; 761 m a.s.l.; Fig. 1A). Upstream of the urban area of Navaluenga, the Alberche river has a length of 70 km in natural flow regime and a watershed of 717 km^2. Bedrock primarily consists of impermeable materials of the Variscian Massif (Orejana et al., 2009) formed by plutonic outcrops (granitoids) and occasional metamorphic rocks (schists and migmatites), favouring the generation of thin soil layers with high potential runoff (Díez, 2001).

Mean annual temperature is 14 °C and mean annual rainfall ranges between 400 and 1200 mm, with November and December normally being the rainiest months. Forests cover the headwaters of the basin and mainly consist of conifers (*Pinus sylvestris* L., *Pinus nigra* Arnold., *Pinus pinaster* Ait. and *Juniperus communis* L.) in the upper and broadleaves in the lower parts (*Quercus pyrenaica* Willd.; *Quercus ilex* L.). Grasslands, scrubs and agricultural soils are also well represented in the catchment. The river corridor is colonized by alder (*Alnus glutinosa* (L.) Gaertn.), ash (*Fraxinus angustifolia* Vahl.), poplar (*Populus* sp.) and willows (*Salix* sp.). Riparian vegetation is easily eliminated during floods and constitutes the main source of woody materials transported to and deposited on the river banks (Fig. 1B).

The village of Navaluenga has a permanent population of 2460 persons, but its population may rise up to 10,000 during the holiday season. Residents from Navaluenga have repeatedly suffered from floods in the past and the oldest reliable documentary records of floods reach back to the mid-18th century (1733, 1739, 1747, 1756, and 1789, 1856, Díez, 2001). In addition, more than 40 written records (i.e. mainly newspaper articles) on floods exist for the past 140 years (Fig. 1B; Díez, 2001). Despite the recurrent flooding at the study site only a short systematic record exists for Navaluenga going back to 1973/1974 when the flow gauge became operational. The mean maximum daily peak discharge (Q_{24}) measured at Navaluenga is 133 m^3 s^{-1} and the upper and lower extremes recorded amount to 522.4 and 15.4 m^3 s^{-1}, respectively.

Dendrogeomorphic analyses and hydraulic simulations were carried out in a reach with a length of 2 km and an averaged slope of 0.003 m/m (see Fig. 1C). This stretch is characterized by anthropogenic interventions and has several hydraulic elements such as bridges, dikes and levees. Vegetated gravel bars and fluvial islands exist at the study reach as well with abundant dendrogeomorphic evidence of past flood events (Fig. 1D). Gravel size measurements carried out along three different transects of the main channel (Fig. 1D) yielded the following data: $D_{50\text{-}T1} = 56.2$ mm; $D_{50\text{-}T2} = 65.7$ mm; $D_{50\text{-}T3} = 97.3$ mm. In addition, field recognition during a low water-stage period has allowed distinction of different morphological features at the study reach, namely sand banks downstream of bridges and different roughness surfaces within the main channel. Visual data from previous studies (Díez, 2001) as well as different aerial and local photographs have been recollected as well and were analyzed to assure that the spatial distribution of the main morphological units did not change during the time period addressed in this study.

3. Material and methods

The approach used in this paper is described conceptually in Fig. 2. The main step of the proposed approach included: (i) a dendrogeomorphic sampling and analysis of scars in riparian trees; (ii) a hydraulic simulation; and (iii) an iterative method to calculate deviation between PSI and modelled water depths.

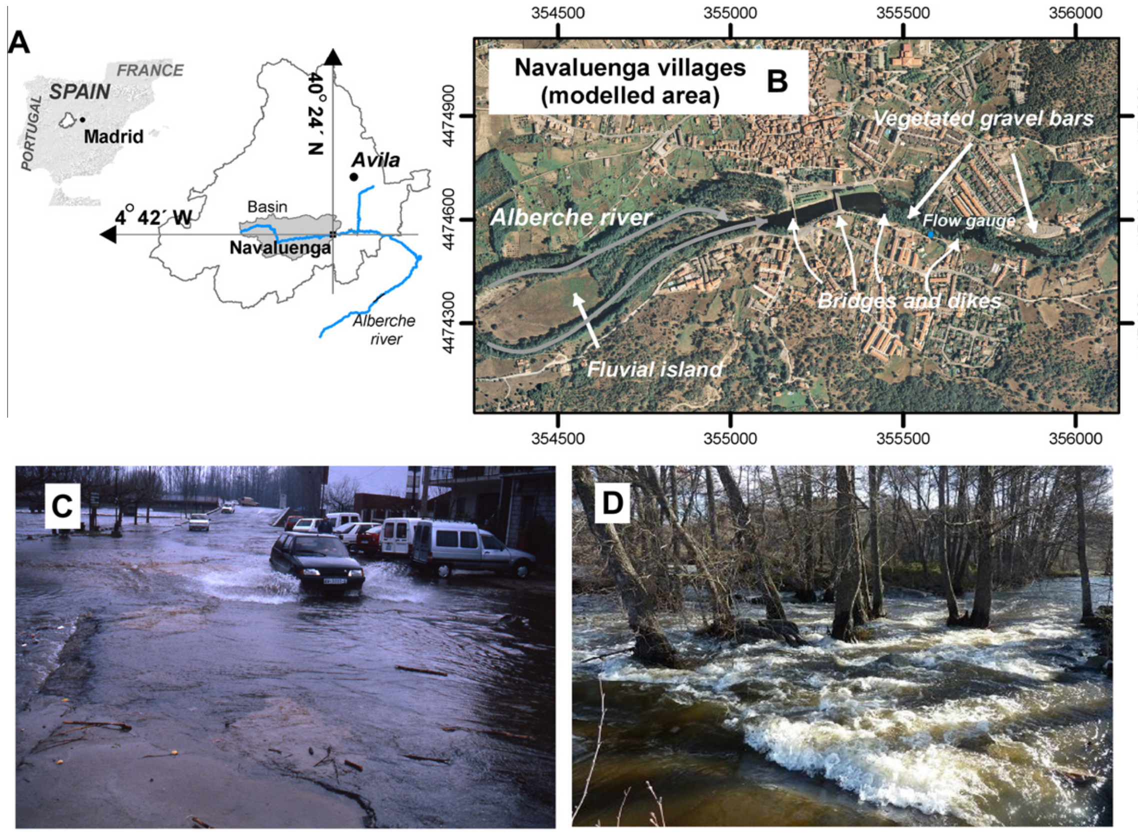

Fig. 1. (A) The Alberche river is located in the Spanish Central System, south of Avila. (B) Location of the modelled area at Navaluenga. (C) Picture from the flood of 8 January 1996. (D) Trees flooded by a recent event (26 February 2010) located on the gravel bars within the modelled area.

3.1. Dendrogeomorphic sampling and analysis of riparian trees

The sampling strategy was based on scars present in trees; both open and overgrown though visible wound were used as palaeostage indicators (PSI) and trees accurately located on the gravel bars and river banks of the modelled area (Baker, 2008; Ballesteros et al., 2010b). Only trees with scars orientated according to the flow direction (Ballesteros et al., 2011) and with meaningful geometry (i.e. excluding unusually large or elongated scars being caused by falling neighbouring trees; Zielonka et al., 2008) were considered. A total of 44 trees with scars inflicted through the impact of woody material during past floods were sampled. In five cases, trees showed multiple wounds corresponding to different floods; whereas in the 39 remaining cases only one impact signal could be identified per tree. For trunks with several scars at different heights, different samples were taken since stems may preserve PSI from different floods. The uppermost point of the highest scar was considered for the estimation of flood stages.

Wedges and increment cores of the overgrowing callus pad of wounded alder (*A. glutinosa* (L.) Gaertn.) and ash trees (*F. angustifolia* Vahl.) were taken with both handsaws and increment borers. In the case of increment cores, samples were taken at the contact between the scar edge and the intact wood tissues to make sure that the entire tree-ring record was obtained (Bollschweiler et al., 2008). In addition, sketches were produced for each tree sampled and geomorphic and geographic positions of each tree were recorded for the subsequent analyses of palaeostage analyses. To this end, a GPS (Trimble 5700) device was used as were field measurements using compass, tape measure and inclinometer.

After field collection, wedges and increment cores were air dried and sanded (up to 400 grit) to facilitate recognition of tree rings (Yanosky and Jarrett, 2002; Stoffel and Bollschweiler, 2008). The dating of flood scars in the tree-ring series was assessed with the help of a binocular stereomicroscope at 10× magnification and flood scar data compiled on skeleton plots (Fritts, 1976).

3.2. Description of the hydraulic model

The hydrodynamic flow model MIKE FLOOD (DHI, 2008) was used to compute water surface elevation at the study site as it allows coupling of the 1D river model MIKE 11 (used for the upstream part of the catchment and until the urban perimeter) with the 2D floodplain model MIKE 21 (used within the urban area) using a vertical link (Stelling and Verwey, 2005) and steady flow simulations. The numerical equations used were based on the conservation of mass and momentum in time and space. By using the 1D flow model upstream Navaluenga we obtained stabilized results of the flow within the urban area, where more obstacles are present, and thus steady results in the downstream part of the modelled perimeter where all benchmarks used for roughness calibration are located. Model boundaries and parameterization required for the model runs were (i) topography, (ii) roughness parameters; and (iii) boundary conditions.

Concerning topography, we carried out a field survey using a differential GPS (Trimble 5700). Cross-sectional areas were produced for the river island area located in the upstream segment of the study reach where the 1D model runs were implemented, whereas in the urban area, a bathymetry was performed with an average density of ~0.3 points m^{-2}. In addition, we used the urban topography (CAD format) at a scale of 1:1000 including contour lines and buildings as well as the most relevant elements in terms of hydraulic modelling (i.e. bridges, levees, dikes, streets) in order to generate

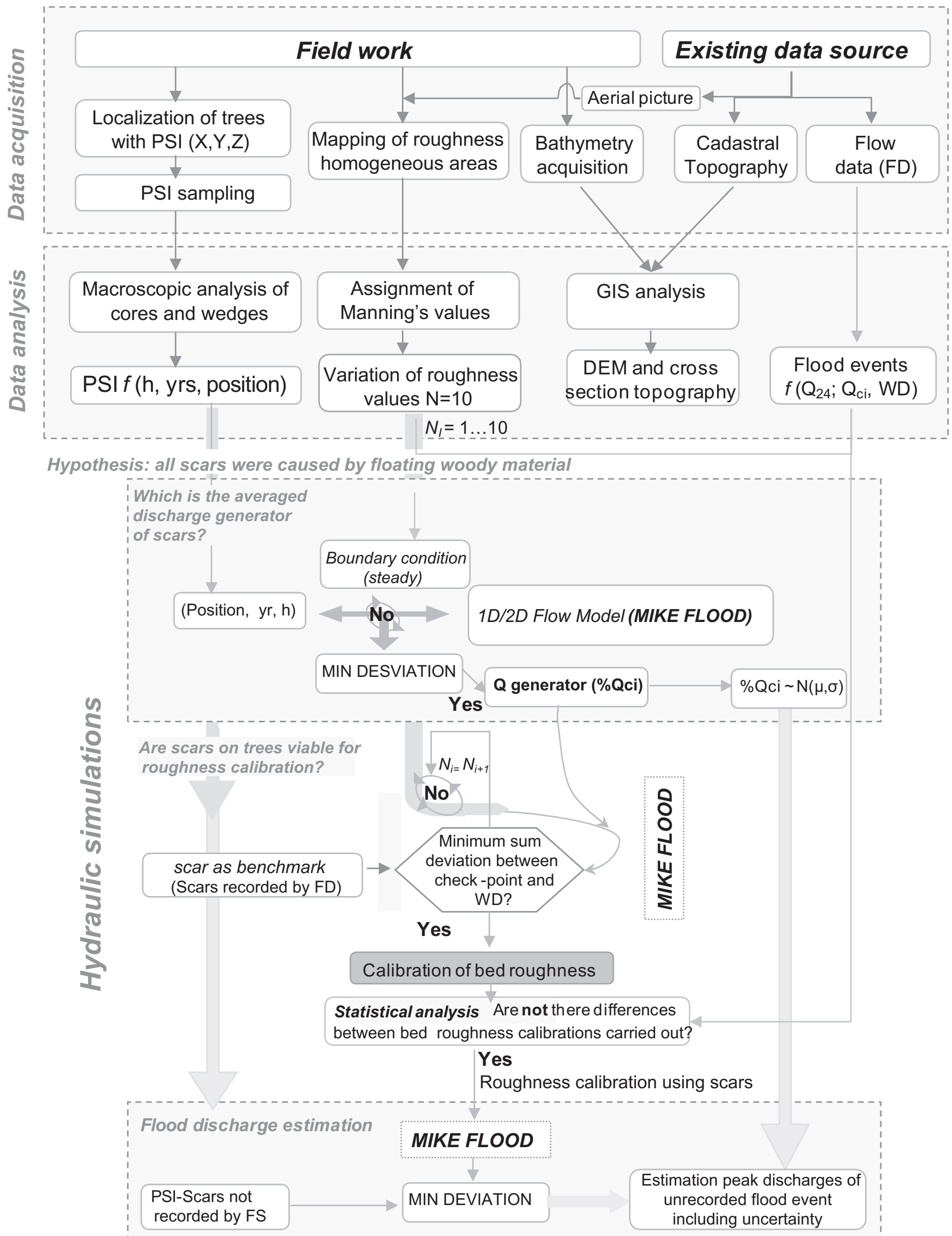

Fig. 2. Methodological flowchart used for the reconstruction of unrecorded flood discharge events based on a spatial roughness calibration using scarred trees. (PSI = palaeostage indicator; yrs = years of the flood event; h = scar heights; GIS = geographical information system; DEM = digital elevation model; Q_{24} = average daily discharge; Q_{ci} = maximum peak discharge; WD = water depth; FD = flow gauge).

a triangulate irregular network (TIN). Topographic data was compiled in ArcGIS 9.2 and an ASCII regular grid (2×2 m) of the study site was derived from a TIN and incorporated to MIKE 21 (Fig. 3).

The roughness coefficient (Manning's n) was obtained from the delineation, both in the channel and the flooding areas, of homogeneous land units in terms of their roughness (RHU, Fig. 4). The observation of different aerial photographs (from 1956 to 2008) and data from previous studies (e.g. Díez, 2001), combined with interviews, leads to the conclusion that morphometry of the main channel did not change significantly over the past 40 years. We therefore assume that roughness values RHU have remained constant in the different units (i.e. gravel bars, fluvial island) identified in the field during the time period considered in this study. This information was placed discretely in cross-sectional areas for the 1D model runs and integrated continuously for the 2D simulations. Each homogeneous unit delimited in the field was digitized using ArcGIS 9.2, and afterwards was assigned a possible rank of values of Manning's n following the criteria defined by Chow (1959; Table 1). In a final step, so as to check the visual assignment of roughness values, we used the Strickler approach (Chang, 1988; $n_S = 0.047 \times (d_{50})^{\frac{1}{6}}$) in three different transects of the main channel.

Boundary conditions for starting the hydraulic calculation have been assigned as normal depths upstream because the channel can be considered longitudinally uniform in the river stretch upstream of the study reach. The link between MIKE 11 and MIKE 21 was carried out by means of lateral links using MIKE FLOOD tools (DHI, 2008).

3.3. Iterative method to calculate deviation between PSI and modelled water depths

An iterative process (Benito and Thorndycraft, 2004) was used in this study to find the best fit between PSI and modelled water depths (WD) for peak discharge available in the flow time series. This approach requires first a definition of bathymetry, floodplain

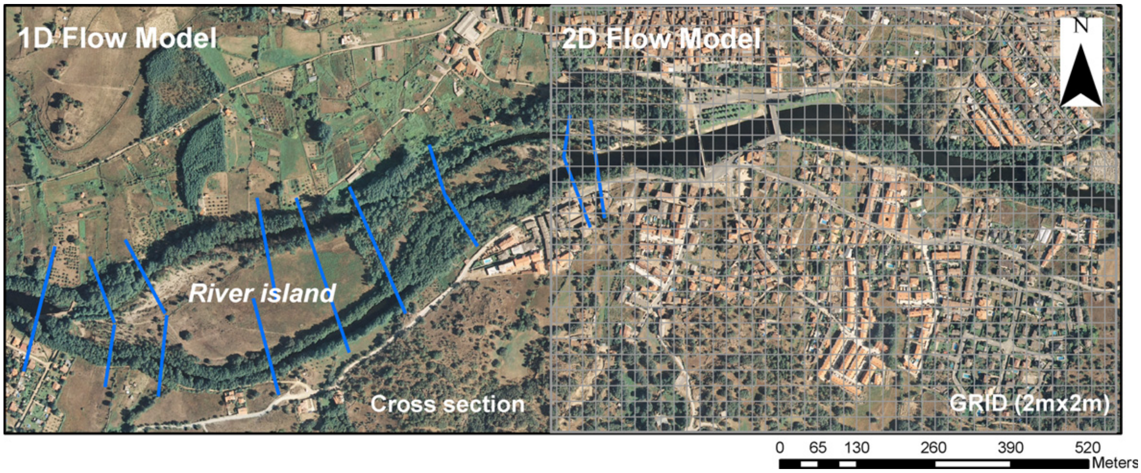

Fig. 3. Overview of the flow model topography at the study reach in Navaluenga.

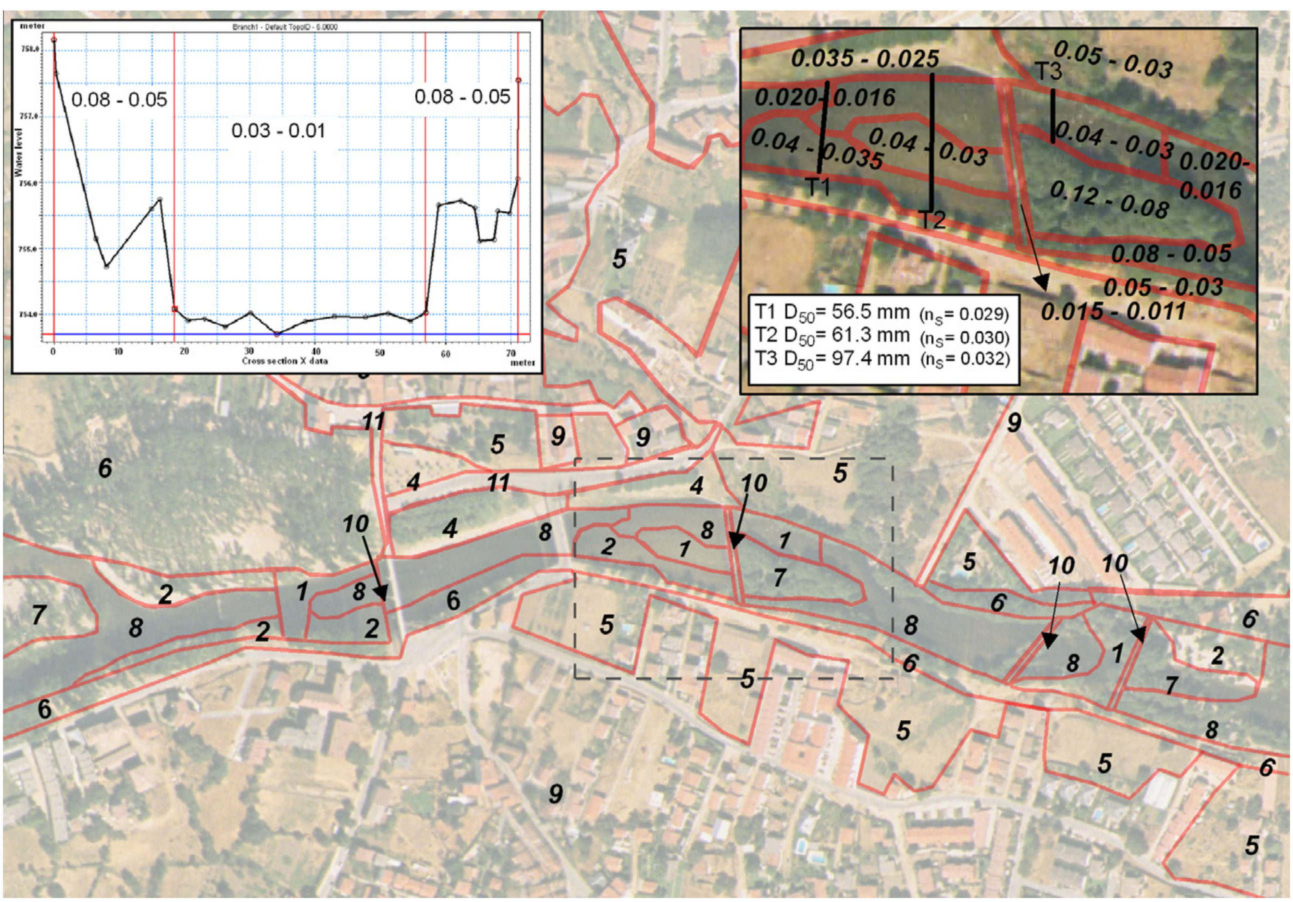

Fig. 4. Details of the roughness homogeneous units (RHU) delimited in the study area and Manning's values used for roughness calibration in cross-sections. Within the scheme located in the right upper part gravel sizes measured and their corresponding manning values (n_s) are presented according to the Strickler equation.

geometry and data on hydraulic properties to solve conservation of mass and momentum equations (Webb and Jarrett, 2002). The deviation between WD and PSI was calculated following the illustration presented in Fig. 5.

For a given peak discharge (Q), the deviation between observed and simulated values is obtained by means of the equation:

$$F(\theta) = Y_{i,m}(\theta_j) - X_{i,m}$$

where $Y_{i,m}$ represents the simulated water depth at point i, for a peak discharge Q of flood event m; roughness coefficients assigned to each homogeneous patch (θ_j) were modified linearly ($j = 1, \ldots, 15$). To be precise, Manning's n values were iteratively varied a 10% within the range of values presented in Table 1. On the other hand, $X_{i,m}$ represents either observed value in terms of maximum scar heights on trees or measured water stages at the flow gauge with regard to the event m.

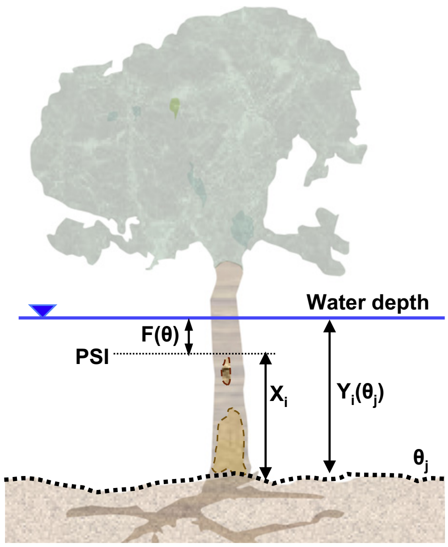

Fig. 5. Assessment of deviations between observed PSI and modelled WD. X_i represents the observed value (i.e. impact scar on tree or rating curve) at position i; and $Y_i(\theta_j)$ the computed water depth for a given roughness θ_j. Deviation between both values is represented by $F(\theta)$.

Table 1
Geomorphic river description and Manning's values assigned to each of the homogeneous patches considered in the hydraulic model.

RHU	Description	(Chow, 1959) class	Rank Manning's values	
			Max	Min
1	Clean and straight main channel with stone and weed	1b	0.04	0.03
2	Clean main channel with more weeds and stones	1d	0.035	0.04
3	Clean main channel with more and greater stones	1f	0.06	0.045
4	Short grass on floodplain	3a-1	0.035	0.025
5	High grass on floodplain	3a-2	0.05	0.03
6	Trees on cleared floodplain with heavy growth of sprouts	3d-3	0.08	0.05
7	Same than above (HU = 6) but with a few down trees, little undergrowth, flood stage below branches	3d-4	0.12	0.08
8	Uniform and clean earth dredged channel	4a-1	0.02	0.016
9	Cement	5a-1	0.013	0.01
10	Mortar	5a-2	0.015	0.011
11	Smooth Asphalt	5i	0.015	0.013

3.3.1. Assessing the peak discharge generating impact scars on trees

One of the principal sources of error in unrecorded flood discharge estimates results from the relationship between PSI and actual WD. Discrepancies between PSI and WD may stem from (i) difficulties in determining the position of the hydrograph at which scars are being inflicted to trees, especially in fluvial system with moderate or larger hydrologic response times (i.e. in floating wood dominated catchments); (ii) an ignorance of the real water depth in systems where scars are inflicted by sediments (i.e. in bedload transport dominated systems). In this study, we initially hypothesize that scars on trees are caused almost exclusively by the impact of floating wood, and that uncertainties would therefore stem from the ignorance of the timing of scar infliction in the hydrograph ordinate. The initial assumption is based on the large availability of large wood, the densely vegetated banks existing in the study area (see Fig. 1C), and field observation during floods.

In a first step, we estimated the average generator peak discharge (Q_{gen}) of scars for each of the floods recorded by the local flow gauge. In this phase, the roughness calibration of the hydraulic model was performed using Manning's values within the ranges defined in Table 1 and by means of the rating curve (which is updated on a yearly basis) of the flow gauge provided by the Tagus Water Authority. Thereafter, the hydraulic model was iteratively run for several peak discharges until it was possible to accurately define Q_{gen} as the average of each peak discharge that minimizes the sum of deviations $F(\theta)$ of scars corresponding to a specific flood. Finally, the ratio Q_{gen}/Q_{ci} of each flood event was treated in a calculus sheet to report the average ($Q_{gen\text{-}MED}$) as well as both the minimum Q_{gen} ($Q_{gen\text{-}MIN}$) and maximum Q_{gen} ($Q_{gen\text{-}MAX}$) of the extreme values at a 95% interval confidence level.

3.3.2. Calibrating floodplain roughness with scar on trees

PSIs have been widely used for peak discharge estimation in the past. However, there is an uncertainty as to whether PSI on trees can be used as a benchmark for floodplain and roughness calibration. An affirmative answer would imply that the highest scar level on trees represents maximum flood stages at a given hydrograph time, which would be in agreement with the hypothesis that injuries are inflicted by floating wood.

To test this hypothesis, we have compared the results obtained via a manual calibration of the roughness using measured values at the flow gauge, and thereafter via the height of the observed PSI. To this purpose, we modelled Q_{gen} of each event by varying linearly (±1/10, decimal steps) and iteratively the Manning's values (associated to each RHU) contained within the range taken into account in Table 1. For the specific case of scars on trees, we defined the calibration as the average of the variation of Manning's values that minimize the deviation between observed scars heights (yielded by a Q_{gen} linked to a flood event) and modelled water depths.

The resulting differences (in decimal steps) between Manning's values obtained from both calibrations (i.e. measured values from the flow gauge and scar height data on tree stems) were analyzed with a non-parametric statistical test (Mann–Whitney W test) at 95 LSD (Sprent and Smeeton, 2001) so as to test the statistical significance of results.

It was assumed that an absence of significant differences between the rating curve and PSI would corroborate our hypothesis that scars on trees were indeed provoked by floating woody materials and that they could therefore be used as a benchmark for the roughness calibration of generator peak discharge.

3.3.3. Estimating peak discharge of the 1970 flood

In a last analytical step, we estimated the peak discharge of an unrecorded flood event dated with dendrogeomorphic techniques but not recorded by the local flow gauge. We applied an iterative method (Webb and Jarrett, 2002) comparing simulated water surface for a given peak discharge and the initial parameterization with the maximum height of PSI in a trial-and-error approach.

Since data on roughness calibration is available for this event, three possible roughness scenarios have been taken into account based on results obtained from the modelling of events where discharge data was available. These scenarios consider 95% of the population of different calibrated Manniné's values for each flood as follows: (i) a mean scenario representing an average of Manning's values minimizing PSI and water depth of all events modelled with known discharge ($M_{\text{-A}}$); (ii) a low scenario where Manning's values of the population correspond to the percentile 2.5 ($M_{\text{-L}}$); and (iii) a high scenario where Manniné's values of the population correspond to the percentile 97.5 ($M_{\text{-H}}$).

Based on these scenarios, three possible Q_{gen} values were obtained (i.e. $Q_{gen\text{-}MED}$; $Q_{gen\text{-}MIN}$ and $Q_{gen\text{-}MAX}$) allowing to infer a probable maximum peak discharge by means of the relationship between Q_{gen} and Q_{ci} for 95% of the distribution values.

4. Results

4.1. Scar on trees as PSI and their correspondence with flow time series

The dating of tree scars on increment cores and wedges allowed identification of eight floods covering the past 40 years, namely 2005 (seven impact scars), 2003 (4), 2002 (7), 2000 (8), 1996 (6), 1993 (9), 1989 (6), and 1970 (2). The spatial distribution of all sampled trees (with dates of flood scars) as well as the flow gauge station is provided in Fig. 6. The illustration also shows that the flow gauge is located between two vegetated gravel bars that have been sampled, implying that differences in data between the flow gauge station and PSI should be minimal. In addition, trees sampled are located in the lower part of the reach simulated with the 2D model and within the active channel.

Table 2 shows that in seven cases, the scars are related to recorded events by the flow gauge (2005, 2003, 2002, 2000, 1996, 1993, and 1989). In addition, dendrogeomorphic data points to a flood in 1970 which is before the flow gauge was installed at the study reach (i.e. station operational since 1973/1974). Table 2 also provides data on water stages measured by the flow gauge and data from PSI as observed via scars on trees. For the 1989 flood event, data on maximum peak discharge (Q_{ci}) is missing, but linear regression between average daily discharge recorded (Q_{24}) and Q_{ci} ($Q_{ci} = 2.0843 \times Q_{24} + 17.281$; $r^2 = 0.92$) allowed however estimation of Q_{ci} to 1168.6 $m^3\ s^{-1}$, representing the largest Q_{24} recorded by the flow gauge since 1972/1973.

4.2. Relationship between the generator peak discharge based on scar heights and flood magnitude

Table 3 shows data on the generator peak discharge based on scar heights (Q_{gen}), results on the deviation between WSP and PSI and the ratio Q_{gen}/Q_{ci}. Peak discharge values obtained after

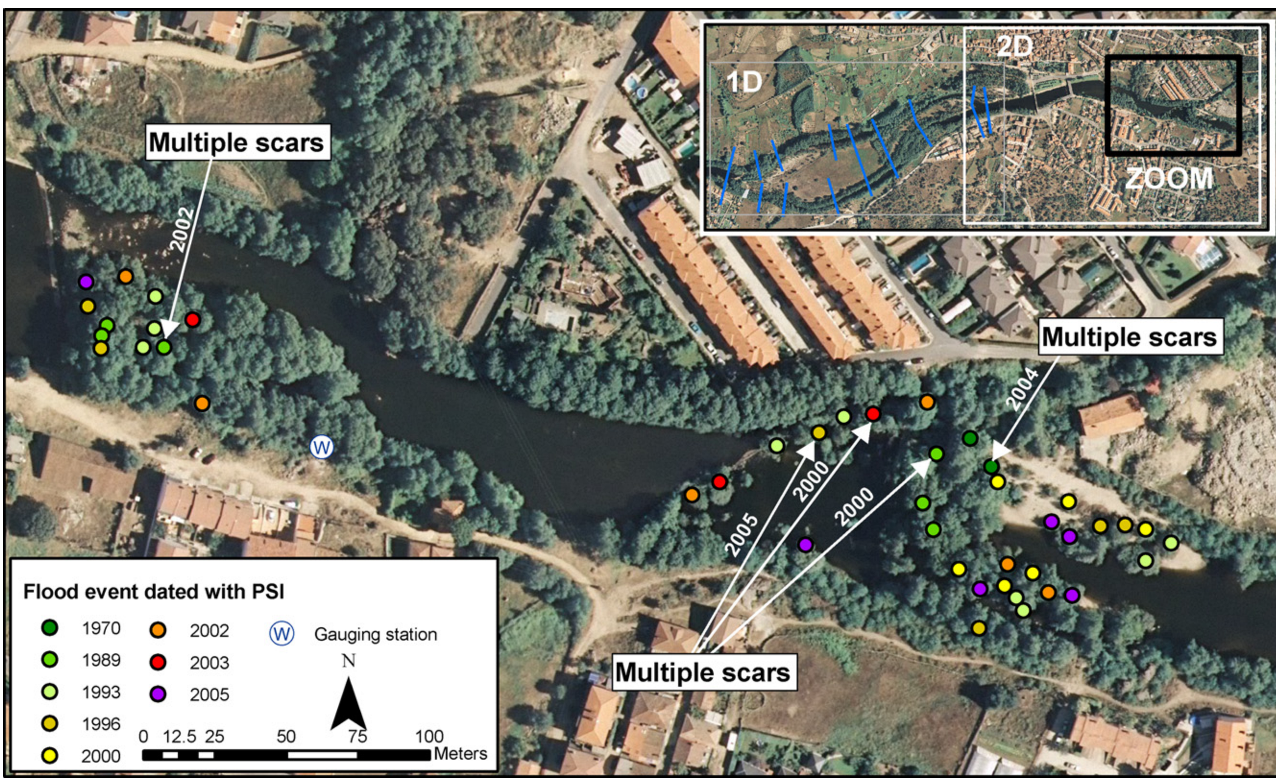

Fig. 6. Geographic distribution of trees selected and dated scars within the modelled study reach.

Table 2
Relationship between scar height with respect to surface, peak discharge and water depth at the flow gauge station (*) Q_{ci} is estimated based on the relationship between Q_{24} and Q_{ci} of the gauge record.

Flood event	Data from flow gauge		Palaeostage indicator (PSI; cm)										μ	σ
	Q_{ci}-m^3/s	Q_{24}-m^3/s	cm	#1	#2	#3	#4	#5	#6	#7	#8	#9		
2005	196.4	196.4	179	174	140	155	175	70	330	100	–	–	163	83
2003	177.5	78.4	156	135	140	80	120	–	–	–	–	–	118	27
2002	487.5	269.6	224	95	126	150	180	140	115	–	–	–	133	26
2000	532.7	201.8	204	80	220	170	236	230	160	90	–	–	169	64
1996	730.4	398.8	257	187	130	150	105	160	200	–	–	–	155	35
1993	792.8	344.9	210	85	108	210	160	160	120	110	160	170	142	39
1989	1168.6*	552.4	–	126	187	145	270	225	180	–	–	–	188	52
1970	–	–	–	260	240	–	–	–	–	–	–	–	250	14

Table 3
Results and ratios obtained for the generator peak discharge based on scar height data, presented with an interval confidence level of 95%.

Flood event	Data				Results		
	Q_{ci}	Q_{24}	Q_{gen}	σ	Q_{gen}/Q_{ci} (%)	95% ICL	
						Lower	Upper
2005	196.4	107.5	115.2	55.6	58.6	35.7	81.6
2003	177.5	78.8	114.3	56.8	64.4	34.0	94.8
2002	487.5	269.6	163.4	31.0	33.5	19.8	47.2
2000	532.7	201.8	202.5	15.0	38.1	30.8	45.3
1996	730.4	398.8	211.1	6.4	28.9	24.3	33.5
1993	792.8	344.9	181.9	11.3	23.0	17.3	28.7
1989	1168.6	552.4	257.3	10.4	23.4	17.2	29.6

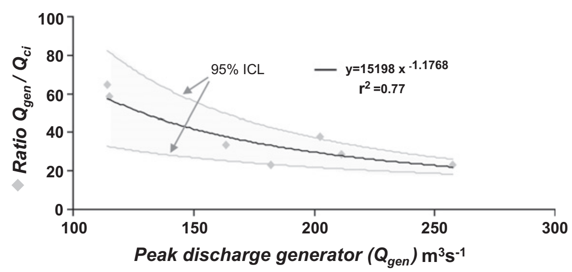

Fig. 7. Relationship between Q_{ci} and Q_{gen} (expressed as% of Q_{ci}) for each of the flood events analyzed.

simulation vary between 114.3 $m^3\,s^{-1}$ for the smallest flood in 2003 and 257.3 $m^3\,s^{-1}$ for the largest flood in 1989. Fig. 7 illustrates that the ratio Q_{gen}/Q_{ci} is between 64.4 and 23% and that the ratio is inversely related with flood magnitude.

Data can be divided in two groups showing different degrees of variability. Despite the similar number of samples in both groups, the variability obtained for the Q_{gen} estimates was smaller (∼9%; mean sample depth = 7) for larger (i.e. 1996, 1993, and 1989) than for smaller (i.e. 2000, 2002 2003, and 2005) floods where variability was almost 39% (mean sample depth = 6). Fig. 6 provides values for the ratio Q_{gen}/Q_{ci} for each flood at a confidence interval level of 95%. The equations describing the relationship between Q_{gen} and Q_{ci} as well as the corresponding correlation coefficients are as follows:

$y = 15198 \cdot x^{-1.1769}$ ($r^2 = 0.77$) for the average results;
$y = 66936 \cdot x^{-1.414}$ ($r^2 = 0.83$) for the upper bound;
$y = 941.9 \cdot x^{-0.7093}$ ($r^2 = 0.48$) for the lower bound;
where y represents the ratio Q_{gen}/Q_{ci} and x represents the Q_{gen}.

4.3. Roughness calibration with PSI

The scar heights observed on the tree trunks reasonably fit water depths measured at the flow gauge station. The calibration procedure using the flow gauge record (systematic data) reported averaged Manning's values which were ∼68% lower than the mean values of the range which was previously defined in Table 1. On the other hand, the calibration procedure using scar heights (non-systematic data) reported average Manning's values which were ∼30% lower than the mean value of the range previously defined in Table 4. The difference between both calibrations was 38.5 ± 63%, which can be translated into an averaged difference in water depths of 8.3 ± 13.8 cm. The non-parametric test yields a p-value = 0.3689 (>0.05), indicating that there is no significant difference between the mean values of the two datasets and that the distribution of scar height values and maximum flood discharge measured at the flow gauge are similar. Based on these

Table 4
Differences between Manning's increment steps minimizing differences between flow gauge data and scar height measurements. (*) Each increment step, resulting to divided Manning's value range of each homogeneous unit between 10, represents a difference in water depth by ∼2.1 ± 0.4 cm (r^2 = 0.9).

Flood event	Manning's values (*) (percentage of the defined range, see Table 1)		Difference (%)
	PSI (scar)	Flow gauge records	
2005	+20	−90	110
2003	−90	−70	20
2002	−140	−80	60
2000	0	−60	60
1996	+30	−60	90
1993	−70	−80	10
1989	+40	−40	80
Average	−30	−68.5	38.5
Standard deviation	69.7	16.7	63.0
Percentile 97.5	40	−90	110
Percentile 2.75	−140	−40	10
Average rank	85.7	64.2	
Mann–Whitney W	17		
W test p-value	0.3689		

results, one can also deduce that scars on trees were indeed generated by floating woody materials and near the water surface of Q_{gen}.

Based on 95% of the data, we obtain a value corresponding to the upper bound (97.5 percentile) $M_{\text{-MAX}}$ = 40 when scars are considered a benchmark for roughness calibration and −90 when compared with the flow time series from the systematic gauge record. In contrast, values corresponding to the lower bound (2.5 percentile; Table 4) are $M_{\text{-MIN}}$ = −140 for scar heights on trees and −40 for the flow gauge record.

Fig. 8 shows the roughness values (i.e. increment steps in relation to the reference value 0) corresponding to the minimum deviation for both scar height data and the rating curve as well as their relationship with Q_{ci} for each of the floods. The smallest deviation between scar height and flow gauge data was observed for the 1993 flood (i.e. after the large 1989 flood); the largest deviation is noted for the 2005 event (i.e. following floods with much smaller magnitudes in 2002 and 2003). This observation might point to a possible control of hydrological dynamics of the Alberche river on channel roughness.

4.4. Estimation of 1970 flood event

For the flood event dated to 1970 with dendrogeomorphic techniques, the computed peak discharge that minimizes deviation between scar heights on trees and water stage (Q_{gen}) was

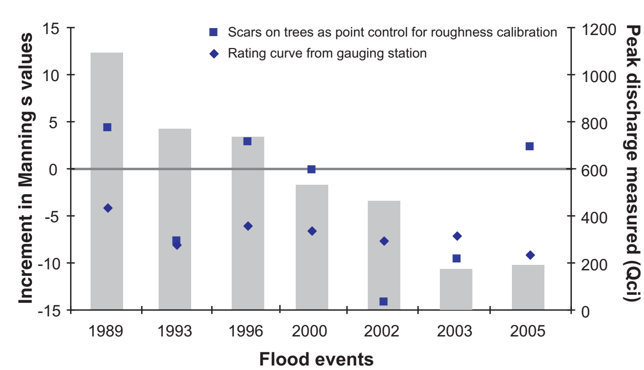

Fig. 8. Variability of increments of Mannings's value steps matching the rating curve and using PSI, as well as their relation with flood magnitude as measured at the flow gauge station.

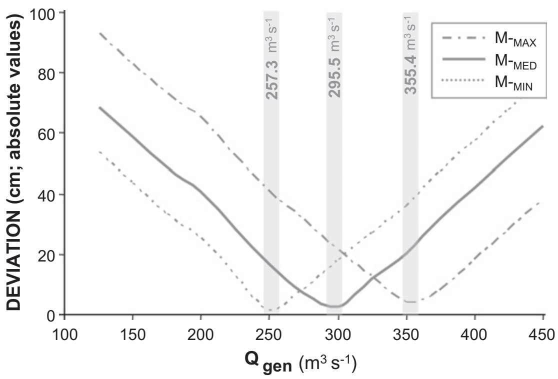

Fig. 9. Peak discharge corresponding to the three scenarios $M_{\text{-MIN}}$, $M_{\text{-MED}}$, and $M_{\text{-MAX}}$ chosen for analysis and based on a roughness calibration with dendrogeomorphic data minimizing deviation with scar heights on trees for the 1970 flood event.

Table 5
Peak discharge obtained for the 1970 flood event considering variability due to floodplain roughness and uncertainties in Q_{gen}.

1970 flood event	Peak discharge estimation (Q_{ci}, m^3 s^{-1}) (interval confidence level 95%)		
	Upper bound	Medium bound	Lower bound
Scenario $M_{\text{-MIN}}$	1400.1	1162.1	984.3
Scenario $M_{\text{-MED}}$	1768.7	1565.0	1369.2
Scenario $M_{\text{-MAX}}$	2427.1	2341.8	2140.8
Average	1865.3 ± 520.2	1689.6 ± 599.6	1498.1 ± 588.9

257.3 m^3 s^{-1} for $M_{\text{-MIN}}$, 295.5 m^3 s^{-1} for $M_{\text{-MED}}$, and 355.4 m^3 s^{-1} for $M_{\text{-MAX}}$ (Fig. 9).

Table 5 provides the Q_{ci} values obtained for the 1970 flood and is based on the relationships established in the previous sections (see Section 4.2) for those floods with scar height and flow gauge data. Peak discharge of the 1970 flood ranges from 1498.1 to 1865.3 m^3 s^{-1}, with a mean of 1684.3 m^3 s^{-1} and a mean dispersion of 519.2 m^3 s^{-1}, representing an uncertainty in the estimation of 30.8%. The values obtained for the 1970 flood therefore suggest a flood which would have been 53% bigger than the largest flood on record.

5. Discussion

5.1. Reliability of scars on trees for roughness calibration

The most important and novel issue addressed in this paper was the use of scars on trees as control for the calibration of floodplain roughness in a hydraulic model. To this end, we analyzed 44 trees presenting 49 scars on their stems associated to eight flood events covering the past 40 years (i.e. 1970, 1989, 1993, 1996, 2000, 2002, 2003, and 2005).

We have hypothesized and demonstrated that scars were inflicted by woody materials, implying that scars heights represent maximum water depths at a given time during the flood. This result allowed both to improve knowledge of scar genesis processes at the study site and consideration of scars as benchmarks for roughness calibration.

Our initial hypothesis is supported by a non-parametric test indicating that differences (p-value > 0.05) between scar heights on trees and water stage given by the rating curve at the flow gauge are not statistically significant. As a consequence, average scar heights of each flood event fit adequately with the water surface derived from Q_{gen} recorded at the flow gauge. Deviations between water depth (considering roughness calibration and using the rating curve) and scar heights on trees (as a benchmark) was less than 20%; our results are thus in concert with observations by Dawdy and Motayed (1979), O'Connor and Webb (1988) or Wohl (1998) who used peak discharge estimates based on different PSI in channels with gradients <0.01.

Initial delimitation of HUR and associated Manning's values were checked in this study at three transects with the Strickler equation, and differences between the calibration procedures could be related to the static dissipative behaviour of the river channel considered, as Manning's values may vary according to different flow depths and as a consequence of relative submergence with respect to sediment size and vegetation height (Chow, 1959; Dingman, 2009). In addition, differences may also related to the accuracy of bathymetry between the flow gauge and tree locations at each cross-section.

Another source of difference between the calibrations could be related to the observed dispersion of Q_{gen} estimations. Our data indicates smaller deviation (~9 m^3 s^{-1}) for larger events (i.e. 1989, 1993, and 1996) and larger deviations for smaller events (i.e. 2000, 2002, 2003, and 2005) where deviations accounted for ~39 m^3 s^{-1}. Moreover, there is an apparent threshold in Q_{gen} bounded between 114.3 and 257.3 m^3 s^{-1}, presumably reflecting channel flow efficiency (Chow, 1959; Chanson, 2004) as well as the existence of a transport domain dominated by woody materials. In fact, we believe that the minimum peak discharge needed to mobilize most available woody materials could be related to bankfull stage events, which are estimated to 195–340 m^3 s^{-1} (CEDEX, 1994) in this stream.

Given that the Alberche river would be represented with a cross-section of the river, an increment in peak discharge during smaller events, characterized by a flood occupying the bankfull area, will be sudden, result in a sudden increase in water depth and thus explain major deviations between observed scar heights and flow gauge data and a higher Q_{gen}/Q_{ci} ratio. By contrast, a similar increment in peak discharge will only provoke a minimal increase in water depth during larger floods since the wetted perimeter will be much bigger and deviations between observed scar heights and flow gauge data much smaller, as will be the Q_{gen}/Q_{ci} ratios.

In previous PSI studies based on scars on trees (Gottesfeld, 1996; Yanosky and Jarrett, 2002; Ballesteros et al., 2011), the deviation between scar heights observed on trees and maximum flood stages seemed to have been influenced by the prevailing hydraulic conditions. In addition, these reconstruction provided acceptable data for unrecorded floods regardless of the nature of material (sediments, woody materials) transported by the event. In this study, however, scars were exclusively induced by woody materials and thus indicate maximum stages reached at a given time of the flood. Our data also shows quite clearly that uncertainties between peak discharge estimated with scars (Q_{gen}) and maximum discharge are directly related to flood magnitude (35.6–77% in the present case, see Table 3), which has important consequences for the reconstruction of large floods. Pictures and video records taken during the 2010 event and post-event field visits reinforce our initial hypothesis (Fig. 10).

The geomorphic pattern of the river and existing hydraulic structures also affect transport of sediments and woody materials during floods. Several gravel bars or heavily vegetated banks are located upstream of the study reach and presumably constitute an important source of sediment and woody materials (Curran, 2010; Malik, 2006) during floods. The existence of different smaller dykes reduces sediment transport (i.e. gravels and smaller boulders) in the case of limited discharge. Decaying riparian vegetation as well as the vegetation present on the bars or banks provides additional sources of material which can easily be mobilized when the flood exceeds the bankfull stage level (Ehrman and Lamberti,

Fig. 10. Woody debris observed around the stem base of trees after the 2010 flood event.

1992; Cordova et al., 2007). Moreover, the operation of small dykes also allows to retain large sediments transported during a flood whereas floating woody materials can overflow these structures without difficulty. On the other hand, the unstable nature of large floating wood and its potential for being suddenly transported (Hupp and Osterkamp, 1996; Gurnell and Sweet, 1998; Tabacchi et al., 2000; Steiger et al., 2005; MacVicar et al., 2009) could also explain the apparent threshold observed in the Q_{gen} values with increasing flood magnitude.

5.2. Flood discharge estimation and its impact on flood frequency analysis

The second objective of this study was to address and quantify uncertainty related to floodplain roughness in discharge estimates using data obtained with dendrogeomorphic approaches. As the Navaluenga flow gauge record reaches only back to 1972/1973, an assessment of floodplain roughness was performed for the unrecorded 1970 flood.

Although the reconstruction of the 1970 flood was based on a rather limited set of scar heights, estimated peak discharge ($1684.3 \pm 519.2\ m^3\ s^{-1}$) is consistent with daily inflow data measured at a dam located 18 km downstream of the study reach where a flood with $512.74\ m^3\ s^{-1}\ 24\ h^{-1}$ was recorded (UF, 1994). The relationship obtained for the 1970 flood is comparable to that of the 1989 flood where the Navaluenga flow gauge recorded $1168\ m^3\ s^{-1}$ and dam inflow was $517.90\ m^3\ s^{-1}\ 24\ h^{-1}$.

Moreover, written records exist for the 1970 flood, reporting serious damage in the areas adjacent to the study reach and thus corroborating the existence of a large flood in the wider Navaluenga region (Díez, 2001; La Vanguardia newspaper, January 13, 1970).

The uncertainty in peak discharge estimate using a roughness calibration derived from dendrogeomorphic data was ~30% and therefore slightly larger than the ±25% reported by Jarrett and England (2002) who used critical depth and slope-conveyance methods for the reconstruction of large flood discharge, but lower than the 40% error occurring in case of large uncertainties in roughness calibration (Kidson et al., 2002). One of the reasons for the uncertainty in our reconstruction certainly reflects the very small number of trees exhibiting scars in 1970 (two samples) at the study reach. While there is additional dendrogeomorphic field evidence for the 1970 and even older flood events, the nature of damage (predominantly tilted or decapitated trees) did not allow for an accurate definition of minimum flood stages and thus prevented their use for magnitude–frequency relationship assessments (Stoffel, 2010). In addition, when observing the ratio Q_{gen}/Q_{ci} obtained from scars on trees located in the lower reaches of the channel (Figs. 5 and 6), we realize the values obtained are not a constant but that they represent an inverse relationship with flood magnitude, thus resulting in much larger uncertainties for larger than for smaller events. As a result, future research should clearly focus on those scarred trees being located farthest from the channel bottom so as to minimize uncertainties in studies focusing on large floods with tree-ring evidence.

Despite these uncertainties, we are convinced that the peak discharge of the 1970 event would represent the largest flood of the recent past and an event bigger than all floods recorded by the flow gauge station since 1972/1973. This observation has important consequences for the definition of flood frequency and magnitude at the study site. A preliminary comparison of peak discharge percentiles obtained by statistical analyses of the systematic records with the discharge estimate of the 1970 flood event using an unweighted GEV function (USWRC, 1981; CEDEX, 2002) clearly points to an increase of flow percentiles associated to each return period (RP, Fig. 11).

As a consequence, our data on the 1970 flood could have major implications for the estimation of flood hazards and associated risk assessments at Navaluenga. The inclusion of the 1970 flood discharge estimate clearly influences percentiles of higher discharge, showing that an assessment of flow percentiles based exclusively on existing systematic data can be a problem for flow gauge stations with short records and thus lead to an underestimation of flood events with large return periods (RP). The graph presented in Fig. 11 is still suffering from a large variability for large RP, but the results obtained in our study could be used as in input to statistical regional flood frequency analysis (Gaume et al., 2010) to improve the knowledge of hydrological processes. As the age of riparian trees at the study site is normally limited to <100 yr, and thus potentially covering RP < 100 years, there is a clear need for the inclusion of older peak discharge estimates derived from sedimentologic records to further improve the local flood frequency analysis for larger RP (Díez, 2001; Benito et al., 2005).

5.3. Implications and limitations for the study of future unrecorded flood events

The methodology presented in this study has the potential to yield distributed roughness calibrations for other regions as well, especially for river stretches with long and complex reaches where the assessment of floods is normally based on only one or a very limited number of systematic benchmarks. This issue has important consequences for the realization of realistic hydraulic models to evaluate potential losses in vulnerable areas as well as for a more accurate estimation of flood discharge based on dendrogeomorphic evidence.

The number of observations and the nature of material (i.e. sediments or woody materials) which is transported by the flood

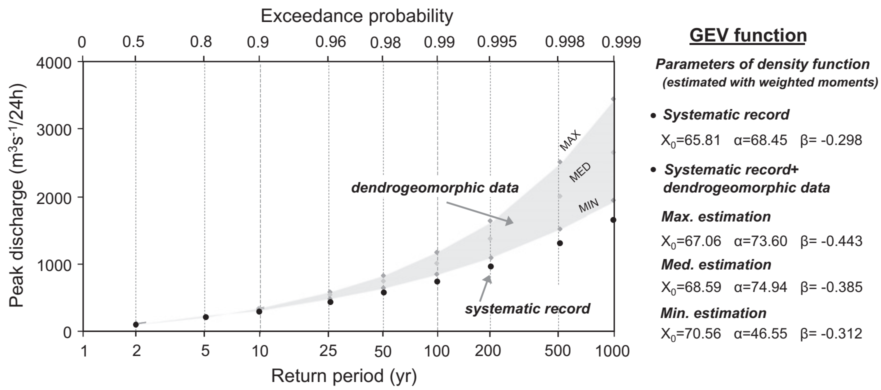

Fig. 11. Results of peak discharge percentiles obtained from the flow gauge station at Navaluenga derived from the systematic record and dendrogeomorphic data. Note the changes in the distribution of values after addition of dendrogeomorphic results of the reconstructed 1970 flood. Statistical analysis was tested by goodness of fit test (p-value > 0.05).

represent the most important parameters for the use of scar data on trees as a benchmark in roughness calibration. At the same time, the main limitation for realistic flood discharge estimation inherent to the methodology presented here is the timing of scar infliction on trees within the hydrograph. We defined this parameter as the ratio Q_{gen}/Q_{ci}, but Q_{ci} data has not always been available. As a result, the methodology presented here can only be applied to other study sites if at least one of the premises listed below are fulfilled:

- Gauged basins: scar on trees can be used to improve a spatially distributed roughness calibration, especially in complex geomorphic sites of the floodplain located far away from the flow gauge. In this context, data from the flow gauge can also be used to explore the Q_{gen}/Q_{ci} ratio. Here, analysis of scar heights induced by floating woody materials will allow determination of the ratio Q_{gen}/Q_{ci}, and at the same time, it can be treated as a random variable defining uncertainty in the unrecorded flood discharge estimation.
- Basins with rainfall data but with flow time series which are not statistically representative: Scars on trees can be used for roughness calibration as well in this case. In addition, previously calibrated and validated hydrological models taking into account the entire catchments will allow for an estimation of the hydrographs, and thus for an assessment of maximum peak discharge (Q_{ci}) of the flood that provoked scars on trees, which can in turn help determination of the relationship (to be treated as a random variable as well).
- Ungauged catchments without rainfall time series: In case that scars on trees are indeed inflicted by floating woody materials, heights of injuries can be used for the validation of roughness values attributed to flooded areas. The reconstruction of palaeoflood events can however have significant uncertainties that will depend on the nature of the catchment, flood magnitude and the position of sampled trees.

Our study belongs to the first group presented, i.e. to the gauged catchments. The ratio Q_{gen}/Q_{ci}, which was determined by eight flood events observed through the presence of tree scars and recorded by the gauge station. It allowed a realistic approach for the determination of floodplain roughness values over the time period covered by the riparian vegetation.

6. Conclusion

This paper has shown that dendrogeomorphic data may represent a very valuable and reliable tool and input for flood hazard analyses, especially in catchments with short gauge records. Noteworthy, in river reaches where riparian vegetation constitutes the main source of material transported by floods, (i) scars on trees are (almost) exclusively inflicted by floating woody materials and (ii) the height distribution of scars on stems has been shown not to be statistically different from discharge data recorded at nearby flow gauge stations. Results of the study also demonstrate that scars on trees can be used as a benchmark for the improvement of roughness calibrations. In addition, scar height data can also be used for peak discharge estimations of older, undocumented floods, which can potentially have major impacts on flood frequency analysis and related frequency-magnitude relationships. Nevertheless, uncertainties remain in estimates of peak discharge in ungauged catchments and a clear need exists for future research to further (i) improve determination of the timing of scar infliction within the hydrograph as well as to (ii) assess their relationship with geomorphic characteristics of the catchment, either through the use of high water marks in the form of sediments lines, floating woody materials or by means of video records of recent floods.

Acknowledgements

This paper was funded in part by the Dendro-Avenidas project (number CGL2007-62063); MASDendro-Avenidas project (number CGL2010-19274) and the MAPHRE foundation. The authors acknowledge the valuable feedbacks from Prof. Marco Borga, and Prof. Vincenzo D'Agostino during the reviewer process as well as the kind collaboration with the Environment Department of Ávila (Castilla-Leon), in particular forester Jose Luis. Galán; the Tagus Water Authority and topographers Luis Fernández y Luis Barca.

References

Aldridge, B.N., Garrett, J.M., 1973. Roughness Coefficients for Stream Channels in Arizona. US Geological Survey Open-File Report, 87 pp.
Antonarakis, A.S., Richards, K.S., Brasington, J., Bithell, M., 2009. Leafless roughness of complex tree morphology using terrestrial LiDAR. Water Resour. Res. 45, W10401.
Arcement Jr., G.J., Schenider, V.R. 1989. Guide for selecting Manning's roughness coefficients for natural channels and flood plains. U.S. Geological Survey Water-Supply Paper 2339. 67 pp. <http://www.fhwa.dot.gov/bridge/wsp2339.pdf>.
Baker, V.R., 2008. Paleoflood hydrology: origin, progress, prospects. Geomorphology 101, 1–13.
Ballesteros, J.A., Stoffel, M., Bodoque, J.M., Bollschweiler, M., Hitz, O., Díez-Herrero, A., 2010a. Changes in wood anatomy in tree rings of *Pinus pinaster* Ait. following wounding by flash floods. Tree-Ring Res. 66 (2), 93–103.
Ballesteros, J.A., Stoffel, M., Bollschweiler, M., Bodoque, J.M., Díez-Herrero, A., 2010b. Flash-flood impacts cause changes in wood anatomy of *Alnus glutinosa*, *Fraxinus angustifolia* and *Quercus pyrenaica*. Tree Physiol. 30 (6), 773–781.
Ballesteros Cánovas, J.A., Eguíbar, M., Bodoque, J.M., Díez-Herrero, A., Stoffel, M., Gutiérrez-Pérez, I., 2011. Estimating flash flood discharge in an ungauged

mountain catchment with 2D hydraulic models and dendrogeomorphic paleostage indicators. Hydrol. Process. 25 (6), 970–979.
Barnes Jr., H.H., 1967. Roughness characteristic of natural channels. U.S. Geological Survey Water-Supply Paper 1849, 213 pp.
Bathurst, J.C., 1993. Flow resistance through the channel network. In: Beven, K., Kirkby, M.J. (Eds.), Channel Network Hydrology. John Wiley & Sons, Chichester, pp. 69–98.
Benito, G., Thorndycraft, V.R., 2004. Systematic, Palaeoflood and Historical Data for the Improvement of flood Risk Estimation, Methodological Guidelines. CSIC, Madrid. 115 pp.
Benito, G., Ouarda, T.B.M., Bárdossy, A., 2005. Applications of palaeoflood hydrology and historical data in flood risk analysis. J. Hydrol. 313 (1–2), 1–2.
Bollschweiler, M., Stoffel, M., Schneuwly, D.M., 2008. Dynamics in debris-flow activity on a forested cone–a case study using different dendroecological approaches. Catena 72, 67–78.
Casas, A., Lane, S.N., Yu, D., Benito, G., 2010. A method for parameterising roughness and topographic sub-grid scale effects in hydraulic modelling from LiDAR data. Hydrol. Earth Syst. Sci. 14, 1567–1579.
CEDEX, 1994. Aspectos prácticos de la definición de la máxima crecida ordinaria. Centro de Estudios y Experimentación de Obras Públicas (MOPTMA). Ministry of Public Works of Spain, Madrid.
CEDEX, 2002. Programa CHAC-Cálculo Hidrometeorológico de Aportaciones y Crecidas. Versión PreALFA03g. Ministry of Public Works of Spain.
Chang, H., 1988. Fluvial Processes in River Engineering. John Wiley, NY. 432.
Chanson, H., 2004. The Hydraulics of Open Channel Flow. Butterworth-Heinemann, Oxford, UK. 630 pp.
Chow, V.T., 1959. Open-channel Hydraulics. McGraw-Hill, New York. 680 pp.
Colmenárez, G., Pardo-Pascual, J.E., Ruiz, L.A., Segura Beltrán, F., 2010. Estudio de la relación de la rugosidad topográfica obtenida a partir de datos LIDAR y GPS con el coeficiente de rugosidad N de Manning. Cuaternario y Geomorfología 24 (1–2), 135–151.
Comiti, F., Cadol, D., Wohl, E.E., 2009. Flow regimes, bed morphology, and flow resistance in self-formed step-pool channels. Water Resour. Res. 45, W04424.
Cook, J.L., 1987. Quantifying peak discharges for historical floods. J. Hydrol. 96, 29–40.
Cordova, J.M., Rosi-Marshall, E.J., Yamamuro, A.M., Lamberti, G.A., 2007. Quantity, controls and functions of large woody debris in Midwestern USA streams. River Res. Appl. 23, 21–33.
Curran, J.C., 2010. Mobility of large woody debris (LWD) jams in a low gradient channel. Geomorphology 116 (3–4), 320–329.
Dawdy, D.R., Motayed, A.K., 1979. Uncertainties in determination of flood profiles. In: McBean, E.A., Hipel, K.W., Unny, T.E. (Eds.), Input for Risk Analysis in Water Systems. Water Resources Publications, Ft. Collins, Colorado, pp. 193–208.
Denlinger, R.P., O'Connell, D.R.H., House, P.K., 2002. Robust determination of stage and discharge: an example from an extreme flood on the Verde River, Arizona. In: House, P.K., Webb, R.H., Baker, V.R., Levish, D.R. (Eds.), Ancient Floods, Modern Hazards: Principles and Applications of Paleoflood Hydrology. Water Science and Application, American Geophysical Union, Washington, DC, pp. 127–146.
DHI, 2008. MIKEFLOOD. 1D-2D Modelling. User Manual. DHI, 108 pp.
Díez, A., 2001. Geomorfología e Hidrología fluvial del río Alberche. Modelos y SIG para la gestión de riberas. PhD thesis. Universidad Complutense de Madrid, Madrid, 587 pp. <http://www.ucm.es/BUCM/tesis/geo/ucm-t25361.pdf>.
Dingman, S.L., 2009. Fluvial Hydraulics. Oxford University Press, Oxford, New York. 570 pp.
Duan, J.G., Nanda, S.K., 2006. Two dimensional depth averaged model simulation of suspended sediment concentration distribution in a groyne field. J. Hydrol. 327, 426–437.
Ehrman, T.P., Lamberti, G.A., 1992. Hydraulic and particular matter retention in a 3rd-order Indiana stream. J. N. Am. Benthol. Soc. 11, 341–349.
Enzel, Y., Ely, L.L., House, P.K., Baker, V.R., Webb, R.H., 1993. Palaeoflood evidence for a natural upper bound to flood magnitudes in the Colorado River basin. Water Resour. Res. 29, 2287–2297.
Ferguson, R., 2007. Flow resistance equations for gravel- and boulder-bed streams. Water Resour. Res. 43, W05427.
Ferguson, R., 2010. Time to abandon the Manning equation? Earth Surf. Proc. Land. 35, 1873–1876.
Fritts, H., 1976. Tree Rings and Climate. Academic Press, New York. 567.
Gaume, E., Gaál, L., Viglione, A., Szolgay, J., Kohnová, S., Blöschl, G., 2010. Bayesian MCMC approach to regional flood frequency analyses involving extraordinary flood events at ungauged sites. J. Hydrol. 394 (1–2), 101–117.
Gottesfeld, A.S., 1996. British Columbia flood scars: maximum flood-stage indicator. Geomorphology 14, 319–325.
Gottesfeld, A.S., Gottesfeld, L.M.J., 1990. Floodplain dynamics of a wandering river, dendrochronology of the Morice River, British Columbia, Canada. Geomorphology 3, 159–179.
Grant, G.E., 1997. Critical flow constrains flow hydraulics in mobile-bed streams: a new hypothesis. Water Resour. Res. 33, 349–358.
Gurnell, A.M., Sweet, R., 1998. The distribution of large woody debris acumulations and pools in relation to woodland stream management in a small, low-gradient stream. Earth Surf. Proc. Land. 23, 1101–1121.
Heritage, G.L., Milan, D.J., 2009. Terrestrial Laser Scanning of grain roughness in a gravel-bed river. Geomorphology 113 (1–2), 4–11.
Hodge, R., Brasington, J., Richards, K., 2009a. In situ characterization of grain-scale fluvial morphology using Terrestrial Laser Scanning. Earth Surf. Proc. Land. 34 (7), 954–968.
Hodge, R., Brasington, J., Richards, K., 2009b. Analysing laser-scanned digital terrain models of gravel bed surfaces: linking morphology to sediment transport processes and hydraulics. Sedimentology 56 (7), 2024–2043.
Hupp, C.R., Osterkamp, W.R., 1996. Riparian vegetation and fluvial geomorphic processes. Geomorphology 14 (4), 277–295.
Jarrett, R.D., England, J.F., 2002. Reliability of paleostage indicators for paleoflood studies. In: House, P.K., Webb, R.H., Baker, V.R., Levish, D.R. (Eds.), Ancient Floods, Modern Hazards: Principles and Applications of Paleoflood Hydrology, Water Science and Application, vol. 5. American Geophysical Union, Washington, D.C., pp. 91–109.
Kidson, R., Richards, K.S., Carling, P.A., 2002. Hydraulic model calibration using a modern flood event: the Mae Chaem River, Thailand. In: Thorndycraft, V.R., Benito, G., Barriendos, M., Llasat, M.C. (Eds.), Palaeoflood, Historical Data and Climatic Variability. CSIC, Barcelona, pp. 171–177.
Kidson, R., Richards, K.S., Carling, P.A., 2005. Reconstructing the ca. 100-year flood in Northern Thailand. Geomorphology 70 (3–4), 279–295.
de Kok, J.L., Grossmann, M., 2010. Large-scale assessment of flood risk and the effects of mitigation measures along the Elbe River. Nat. Hazards. 52 (1), 143–166.
Leandro, J., Chen, A.S., Djordjevic, S., Savic, D.A., 2009. Comparison of 1D/1D and 1D/2D Coupled (Sewer/Surface) Hydraulic Models for Urban Flood Simulation. J. Hydraul. Eng. 135 (6), 495–504.
MacVicar, B., Piegay, H., Henderson, A., Comiti, F., Oberline, C., Pecorari, E., 2009. Quantifying the temporal dynamics of wood in large rivers: field trials of wood surveying, dating, tracking, and monitoring techniques. Earth Surf. Proc. Land. 34 (15), 2031–2046.
Malik, I., 2006. Contribution to understanding the historical evolution of meandering rivers using dendrochronological methods: example of the MaLa Panew River in southern Poland. Earth Surf. Proc. Land. 31, 1227–1245.
O'Connor, J.E., Webb, R.H., 1988. Hydraulic modelling for palaeoflood analysis. In: Baker, V.R., Kochel, R.C., Patton, P.C. (Eds.), Flood Geomorphology. Jhon Wiley and Sons, New York, pp. 393–402.
Orejana, D., Villaseca, C., Perez-Soba, C., López-García, J.A., Billström, K., 2009. The Variscan gabbros from the Spanish Central System: a case for crustal recycling in the sub-continental lithospheric mantle? Lithos 110 (1–4), 262–276.
Roca, M., Martín-Vide, J.P., Moreta, P.J.M., 2008. Modelling a torrential event in a river confluence. J. Hydrol. 364 (3–4), 207–215.
Ruiz-Villanueva, V., Díez-Herrero, A., Stoffel, M., Bollschweiler, M., Bodoque, J.M., Ballesteros, J.A., 2010. Dendrogeomorphic analysis of flash floods in a small ungauged mountain catchment (Central Spain). Geomorphology 118, 383–392.
Simon, A., Bennett, S.J., Neary, V.S., 2004. Riparian vegetation and fluvial geomorphology: problems and opportunities. In: Bennett, S.J., Simon, A. (Eds.), Riparian Vegetation and Fluvial Geomorphology, Water Science and Application 8. Washington DC, 1–10.
Souhar, O., Faure, J.B., 2009. Approach for uncertainty propagation and design in Saint Venant equations via automatic sensitive derivatives applied to Saar River. Can. J. Civil Eng. 36 (7), 1144–1154.
Sprent, P., Smeeton, N.C., 2001. Applied Nonparamentric Statistical Methods. Chapman & Hall/CRC, Boca Raton, London, New York, Washington, D.C.
Steiger, J., Tabacchi, E., Dufour, S., Corenblit, D., Peiry, J.L., 2005. Hydrogeomorphic processes affecting riparian habitat within alluvial channel-floodplain river systems: a review for the temperate zone. River Res. Appl. 21, 719–737.
Stelling, G.S., Verwey, A. 2005. Numerical Flood Simulation. In: Encyclopedia of Hydrological Sciences, vol. 1. John Wiley & Sons Ltd., 257–270.
St. George, S., Nielsen, E., 2003. Palaeoflood records for the Red River, Manitoba, Canada, derived from anatomical tree-ring signatures. Holocene 13 (4), 547–555.
Stoffel, M., 2010. Magnitude-frequency relationships of debris flows–A case study based on field surveys and tree-ring records. Geomorphology 116, 67–76.
Stoffel, M., Wilford, D.J., in press. Hydrogeomorphic processes and vegetation: disturbance, process histories, dependencies and interactions. Earth Surf. Process. Land.
Stoffel, M., Beniston, M., 2006. On the incidence of debris flows from the early Little Ice Age to a future greenhouse climate: a case study from the Swiss Alps. Geophys. Res. Lett. 33, L16404.
Stoffel, M., Bollschweiler, M., 2008. Tree-ring analysis in natural hazards research–an overview. Nat. Hazards Earth Syst. Sci. 8, 187–202.
Stoffel, M., Bollschweiler, M., Butler, D.R., Luckman, B.H., 2010. Tree rings and natural hazards: a state-of-the-art. Springer, Heidelberg, Berlin, New York. 413 pp.
Sudhaus, D., Seidel, J., Bürger, K., Dostal, P., Imbery, F., Mayer, H., Glaser, R., Konold, W., 2008. Discharges of past flood events based on historical river profiles. Hydrol. Earth Syst. Sci. 12, 1201–1209.
Tabacchi, E., Lambs, L., Guilloy, H., Planty Tabachii, A.-M., Muller, E., Décamps, H., 2000. Impacts of riparian vegetation on hydrological processes. Hydrol. Process. 14, 2959–2976.
Tayefi, V., Lane, S.N., Hardy, R.J., Yu, D., 2007. A comparison of one- and two-dimensional approaches to modelling flood inundation over complex upland floodplains. Hydrol. Process. 21 (23), 3190–3202.
Thorndycraft, V.R., Benito, G., Rico, M., Sopeña, A., Sánchez, Y., Casas, A., 2005. A long-term flood discharge record derived from slackwater flood deposits of the Llobregat River, NE Spain. J. Hydrol. 313 (1–2), 16–31.
Tinkler, K.J., 1997. Critical flow in rockbed streams with estimated values for Manning's n. Geomorphology 20, 147–164.
UF, 1994. Datos de caudal de entrada a la presa del Burguillo (Ávila). Electric Company, Internal documentation, Madrid.

USWRC, 1981. Guidelines for Determining Flood Flow Frequency. Bulletin 17B, Water Resour. Council, Washington.
Yanosky, T.M., Jarrett, R.D., 2002. Dendrochronologic evidence for the frequency and magnitud of paloflods. In: House, P.K., Webb, R.H., Baker, V.R., Levish, D.R. (Eds.), Ancient Floods, Modern Hazards: Principles and Applications of Paleoflood Hydrology, Water Science and Application, vol. 5. American Geophysical Union, Washington, D.C, pp. 77–89.
Yen, B.C., 2002. Open channel flow resistence. J. Hydraul. Eng. 128 (1), 20–39.
Webb, R.H., Jarrett, R.D., 2002. One-dimensional estimation techniques for discharges of paleofloods and historical floods. In: House, P.K., Webb, R.H., Baker, V.R., Levish, D.R. (Eds.), Ancient Floods, Modern Hazards: Principles and Applications of Paleoflood Hydrology, Water Science and Application, vol. 5. American Geophysical Union, Washington, D.C., pp. 111–126.
Werner, M.G.F., Hunter, N.M., Bates, P.D., 2005. Identifiably of distributed floodplain roughness values in flood extent estimation. J. Hydrol. 314 (1–4), 139–157.
Wohl, E.E., 1998. Uncertainty in flood estimates associated with roughness coefficient. J. Hydraul. Eng. 124 (2), 219–277.
Zhu, C.J., Zhang, J., 2009. Prediction of roughness coefficient using multivariate forecast model. In: Luo, Q. (Ed.), ETP/IITA World Congress in Applied computing, Computer Science and Computer Engineering. ACC, Sanya, pp. 319–322.
Zielonka, T., Holeksa, J., Ciapala, S., 2008. A reconstruction of flood events using scarred tree in the Tatra Mountains, Poland. Dendrochronologia 26, 173–183.